Received: 8 January 2018 | Revised: 19 July 2018 | Accepted: 14 August 2018

DOI: 10.1002/hipo.23020

WILEY

RESEARCH ARTICLE

Temporal coding and rate remapping: Representation of nonspatial information in the hippocampus

Honi Sanders[1,2] | Daoyun Ji[3] | Takuya Sasaki[4] | Jill K. Leutgeb[4] | Matthew A. Wilson[3] | John E. Lisman[1,5]

[1]Volen Center for Complex Systems, Brandeis University, Waltham, Massachusetts

[2]Neuroscience Program, Brandeis University, Waltham, Massachusetts

[3]Department of Brain and Cognitive Sciences, Picower Institute for Learning and Memory, Massachusetts Institute of Technology, Cambridge, Massachusetts

[4]Division of Biological Sciences, Neurobiology Section and Center for Neural Circuits and Behavior, University of California, San Diego, California

[5]Department of Biology, Brandeis University, Waltham, Massachusetts

Correspondence
Honi Sanders, 43 Vassar Street, Room 46-5233, Cambridge, MA 02139.
Email: honi@mit.edu

Funding information
NSF CRCNS, Grant/Award Number: 1R01DA027807; Walter F. Heiligenberg Professorship; JSPS Postdoctoral Fellowship for Research Abroad; NSF IGERT, Grant/Award Number: DGE-1068620; NIMH, Grant/Award Numbers: R01MH061976, R01MH100349, R01MH102841, F31MH103966

Abstract

Hippocampal place cells represent nonspatial information through a process called rate remapping, which involves a change in the firing rate of a place cell without changes in its spatial specificity. However, many hippocampal phenomena occur on very short time scales over which long-term average firing rates are not an appropriate description of activity. To understand how rate remapping relates to fine-scale temporal firing phenomena, we asked how rate remapping affected burst firing and trial-to-trial spike count variability. In addition, we looked at how rate remapping relates to the theta-frequency oscillations of the hippocampus, which are thought to temporally organize firing on time scales faster than 100 ms. We found that theta phase coding was preserved through changes in firing rate due to rate remapping. Interestingly, rate remapping in CA1 in response to task demands preferentially occurred during the first half of the theta cycle. The other half of the theta cycle contained preferential expression of phase precession, a phenomenon associated with place cell sequences, in agreement with previous results. This difference of place cell coding during different halves of the theta cycle supports recent theoretical suggestions that different processes occur during the two halves of the theta cycle. The differentiation between the halves of the theta cycle was not clear in recordings from CA3 during rate remapping induced by task-irrelevant sensory changes. These findings provide new insight into the way that temporal coding is utilized in the hippocampus and how rate remapping is expressed through that temporal code.

KEYWORDS

overdispersion, phase precession, place cells, theta rhythm, theta sequence

1 | INTRODUCTION

The hippocampus is well known for the location-specific firing of its principal cells, termed "place cells" (O'Keefe, 1976). Place cell firing involves more than a simple representation of the current location of the animal. For example, sequences of place cells corresponding to actual paths through the environment occur during the theta-frequency (6–12 Hz) oscillations that occur during engaged behavior (Buzsaki, 2002). During each ~100 ms theta cycle, the place cell population represents the sequence of upcoming locations in order (Foster & Wilson, 2007; Skaggs, McNaughton, Wilson, & Barnes, 1996). Thus, the function of the hippocampus can only be understood if one takes into consideration temporal coding properties.

In addition to representing spatial sequences, place cells also represent nonspatial in-formation (e.g., sensory: Leutgeb et al., 2005 or task-related Allen, Rawlins, Bannerman, & Csicsvari, 2012). This phenomenon has been described in terms of the effects of nonspatial information on the long-term average firing rates of place cells and thus has been termed "rate remapping". While the preferred response location ("place field") of a given cell does not change with the content of the nonspatial information, the rate at which the place cell fires within the place field can change by an order of magnitude. This phenomenon has generated interest (Schiller et al., 2015) because it bridges the gap between the hippocampal spatial map and the function of the hippocampus in the formation of episodic memory, an essential component of which is nonspatial information (Eichenbaum, Yonelinas, & Ranganath, 2007; Scoville & Milner, 1957). However, studies of

rate remapping thus far have generally examined the long-term average firing rate of place cells over the course of 10 (Leutgeb et al., 2005) or 30 min (Ji & Wilson, 2008), but see (Mankin, Diehl, Sparks, Leutgeb, & Leutgeb, 2015; Mankin et al., 2012) for within-session effects on firing rate. Given that an entire sequence of locations is played out during the ~100 ms theta cycle, rate remapping information associated with individual locations in that sequence must be available on even shorter time scales. To this end, we studied fine-scale temporal aspects of rate remapping, as described in the following paragraphs.

One aspect of fine-scale response properties in the hippocampus is the tendency of cells to fire in high-frequency bursts (Ranck, 1973). These bursts have been experimentally associated with particular input pathways (Bittner et al., 2015; Royer et al., 2012). Theoretical work has suggested that, by modulating the number of spikes that occur within a burst, graded information can be encoded on very fast time scales (Kepecs & Lisman, 2003). Therefore, we looked at whether rate remapping is the result of a change in the number of spikes per burst.

Another aspect of place cell firing that reveals itself on analysis of short time scales is the extreme variability of spike counts on different single passes through a particular location (Fenton & Muller, 1998). This unexplained variability, which is known as "overdispersion", implies that there are hidden variables that affect place cell activity. We examined the possibility that the representation of nonspatial information via rate remapping is the source of this variability.

Interestingly, one theory that has been proposed to explain this excess variability provides an alternative interpretation of rate remapping. It has been shown that, for a task in which an animal must switch between maze and room cues, there are actually separate hippocampal maps for the two reference frames and the hippocampus switches between them in a task-dependent way (Fenton et al., 2010; Kelemen & Fenton, 2016). It has been suggested that this process of map switching may actually be a more general phenomenon that occurs under all conditions and that the hippocampus switches between maps at a frequency of 1–10 Hz (Olypher, L'ansky, & Fenton, 2002; Jackson & Redish, 2007; Jezek, Henriksen, Treves, Moser, & Moser, 2011). According to this suggestion, the excess variability observed in place cell firing is the result of map switches that the experimenter is unaware of and has not accounted for. When averaged over many map switches, changes in probability of firing look like changes in rate of firing. In this way, nonspatial variables could be understood as affecting the probability of inhabiting particular maps instead of as changing a consistent firing rate in a given map. Therefore, we looked at the probability and frequency of firing on time scales short enough to ensure the presence of only a single map.

Another important issue is the expression of rate remapping on a subtheta cycle time scale. The possibility that place cells independently code spatial and nonspatial information is an interesting one, but it runs into potential difficulties. As mentioned above, place cell activity shows organization within the ~100 ms theta cycle. An important aspect of that temporal organization is the phenomenon known as theta phase precession (O'Keefe & Recce, 1993), in which each place cell fires at earlier and earlier theta phase as the animal progresses through its place field (Lisman & Redish, 2009). Theta phase precession is closely related to the phenomenon of theta sequences, but is not exactly the same, as theta phase precession is a single-cell phenomenon whereas theta sequences are an ensemble phenomenon which require learning to stabilize (Feng, Silva, & Foster, 2015). Both of these phenomena may be disrupted by firing rate changes if extra spikes resulting from increased firing rate are distributed at theta phases not corresponding to the position of the animal. We therefore tested whether the rate code of rate remapping interfered with the temporal code of theta phase precession.

In a final set of analyses, we asked the question of whether rate remapping occurs uniformly throughout the theta cycle. This question is of particular interest given theoretical work (Hasselmo, Bodelón, & Wyble, 2002; Sanders, Rennó-Costa, Idiart, & Lisman, 2015) and experimental work (Hyman, Wyble, Goyal, Rossi, & Hasselmo, 2003; Schomburg et al., 2014; Siegle & Wilson, 2014; Zheng, Bieri, Hsiao, & Colgin, 2016) suggesting that different phases of theta have different computational functions. In particular, it was suggested that the first half of theta is concerned with computations about current position, whereas the second half of theta deals with predictions associated with upcoming locations (Sanders et al., 2015). Our results provide support for this classification of function through analysis of the theta phase preference of rate remapping.

We addressed the above questions by analyzing two rich datasets available to us. For one task, rats were trained to run back and forth on a black linear track to receive reward at both ends of the track. On the recording days, comparisons were made between place cell activity on the black track and activity on the same task when the black track surface had been switched out for a white surface. This task is similar to other sensory rate remapping paradigms, for which rate remapping occurs in the CA3 region as well as the downstream CA1 region (Leutgeb et al., 2005). We analyzed recordings from CA3 during this task and refer to this data as the "Sensory/CA3" dataset.

For the other task, recordings of place cells in rats on a nondelay alternation task demonstrate rate remapping between the two trajectories (Ji & Wilson, 2008; Robitsek, White, & Eichenbaum, 2013; Wood, Dudchenko, Robitsek, & Eichenbaum, 2000). On each trial, the rat runs down the central arm of a figure-8 shaped maze. At the end, it can turn either left or right. Reward is given for turning the opposite direction of the previous trial. Neurons with place fields on the central arm rate remap depending on which trial type (from left to right or from right to left) the rat is currently on (Frank, Brown, & Wilson, 2000; Ji & Wilson, 2008; Wood et al., 2000). This rate remapping occurs in CA1 place cells, but not in the upstream CA3 place cells (Ito, Zhang, Witter, Moser, & Moser, 2015). Rate remapping in CA1 is inherited from prefrontal cortex via the thalamus, and the task is not hippocampal dependent, so the rate remapping is a reflection of task information, not a driver of decision-making (Ito et al., 2015). We analyzed recordings from CA1 during this task and refer to this data as the "Internally Generated (IntGen)/CA1" dataset. This task is important to study because the variable being represented in the firing rate of the place cells is internally generated; there are no external cues to differentiate between the trial types.

Because these forms of rate remapping differ in the type of information represented and in the relevant region, they provide an overview of how temporal coding is affected by rate remapping. However, one should be careful not to directly compare the results from

the two datasets, because it is impossible to say whether differences are a result of differences between the brain areas or the result of differences between the tasks.

2 | MATERIALS AND METHODS

All data analysis was performed by HS under the supervision of JEL. Unpublished CA3 data was provided by TS, and collected in the lab of JKL. Unpublished CA1 data was provided by DJ, and collected in the lab of MAW.

2.1 | Sensory/CA3 task data collection

Recording procedures have been described in detail previously (Mankin et al., 2015). All surgical and experimental procedures were approved by the University of California, San Diego IACUC. Three rats (Long-Evans males, 3–5 months old, preoperative weight of 375–485 g) were trained to perform the Sensory/CA3 task after prior training in a spatial working memory task in a radial 8-arm maze for 3 weeks. An electrode assembly that consisted of 14 independently movable tetrodes was implanted above the right hippocampus (4.0 mm posterior and 2.9 mm lateral relative to Bregma).

Two weeks after surgery, access to food was restricted and the rats were maintained at about 85% of the free-feeding body weight. Water was readily available. Animals were trained to run back and forth on a linear track with a black vinyl surface (148 × 7 cm with small sides rising .5 cm above the surface of the arm, 53 cm elevated from the floor) to obtain chocolate milk reward at the ends of the track. The training lasted for 2 days.

Electrophysiological recording started when well-separated units were identified in the hippocampus. LFP recordings were filtered between 1 and 425 Hz. Unit activity was amplified and band-pass filtered at 600 Hz to 6 kHz. Spike waveforms above a trigger threshold (40 μV) were recorded at 32 kHz and sorted manually offline (A.D. Redish, http://redishlab.neuroscience.umn.edu/MClust/MClust.html.) Autocorrelation and crosscorrelation functions were used as additional separation criteria. CA3 cells with an average firing rate of less than 3 Hz and waveforms longer than 200 μs were considered to be putative excitatory cells and included in analysis. The animals' positions were tracked with two infrared diodes mounted over the animal's head and sampled at 30 Hz.

Each recording day consisted of four 10 min long sessions with an intertrial interval of 5 min. During the first and fourth session, animals performed the task on the familiar black track. During the second and third sessions, the black surface of the track was switched out for a white vinyl surface. The animals were recorded on 2 days each.

2.2 | Internal/CA1 task data collection

The experimental procedure has been described previously (Ji & Wilson, 2008). Briefly, rats (Long-Evans males, 5–8 months old) were trained on a figure-8 shaped maze for about 2–3 weeks, for about 30 min each day. The animal was rewarded with chocolate sprinkles every time he alternated between two trajectories that shared the same central arm. After the animal achieved a performance criterion of at least 80% accuracy, a tetrode array containing 18 tetrodes was surgically implanted targeting the right dorsal CA1 (coordinates: 4.1 mm posterior and 2.2 mm lateral relative to Bregma). Tetrodes were slowly moved to the CA1 pyramidal layer during the 2–3 weeks after the surgery. One week after surgery, rats were retrained on the figure-8 alternation task.

Recording started once clusters of spikes were stabilized and the animal's performance reached the presurgery performance level. Spikes were identified by a threshold of ~70 μV, sampled at 32 kHz, and manually sorted offline using the spike amplitudes across four tetrode channels (XClust, M. Wilson). Local field potentials (LFPs) were sampled at 2 kHz. The animal's positions were tracked with two infrared diodes mounted over the animal's head and sampled at 30 Hz.

The data analyzed here were acquired from three rats while they were performing the figure-8 alternation task. The rats later performed a trajectory-switching task (Ji & Wilson, 2008), but the data were not included in the analysis here.

2.3 | Data analysis: Technical definitions

Place cells were defined as having overall firing rate >.02 and <4 Hz.

Place fields were defined as areas where the firing rate of the cell was greater than 10% of the maximum firing rate of that cell. Place fields with gaps that were smaller than 10 cm and less than 1/5 of the total size of the place field were merged into a single place field. Place fields with fewer than 5 total spikes, lower than .5 Hz firing rate, or smaller than 3 cm (a single spatial bin) were removed.

For the CA1 dataset, place cells with place fields on the central arm were considered as potential remappers and included for subsequent analysis (74/198 cells). Of those, one cell had two place fields on the central arm for a total of 75 place fields analyzed in Figure 1c. Of those place fields, 44 had a firing rate ≥.5 Hz and 5 or more spikes fired for the low firing rate condition and therefore had sufficient firing for the comparisons shown in all following figures (Figures 2–6).

For the CA3 dataset, we restricted our analysis to locations sufficiently far from the edge of the track so that data would not be confounded with reward site activity. We defined reward locations manually by excluding areas close to the edge of the track, where the animal had low velocity. These locations corresponded to a region of ~10–20 cm at each edge of the track. We calculated place fields separately for rightward passes and leftward passes, as we found independence of place cell activity for opposite directions of motion (data not shown, see also Markus et al., 1995). For the CA3 data, of 154 units recorded, 37 had place fields on leftward passes and 33 had place fields on rightward passes. Of those, 17 cells had multiple place fields for a total of 87 place fields analyzed in Figure 1d. Of those, 32 place fields had a firing rate ≥.5 Hz and 5 or more spikes fired for the low firing rate condition and therefore had sufficient firing for the comparisons shown in all following figures (Figures 2–6).

Theta was defined by filtering the raw LFP trace, as measured at the local pyramidal cell layer, between 6 and 10 Hz. Local maxima (peaks) were defined as 0 phase, and other phases were linear interpolation between consecutive peaks.

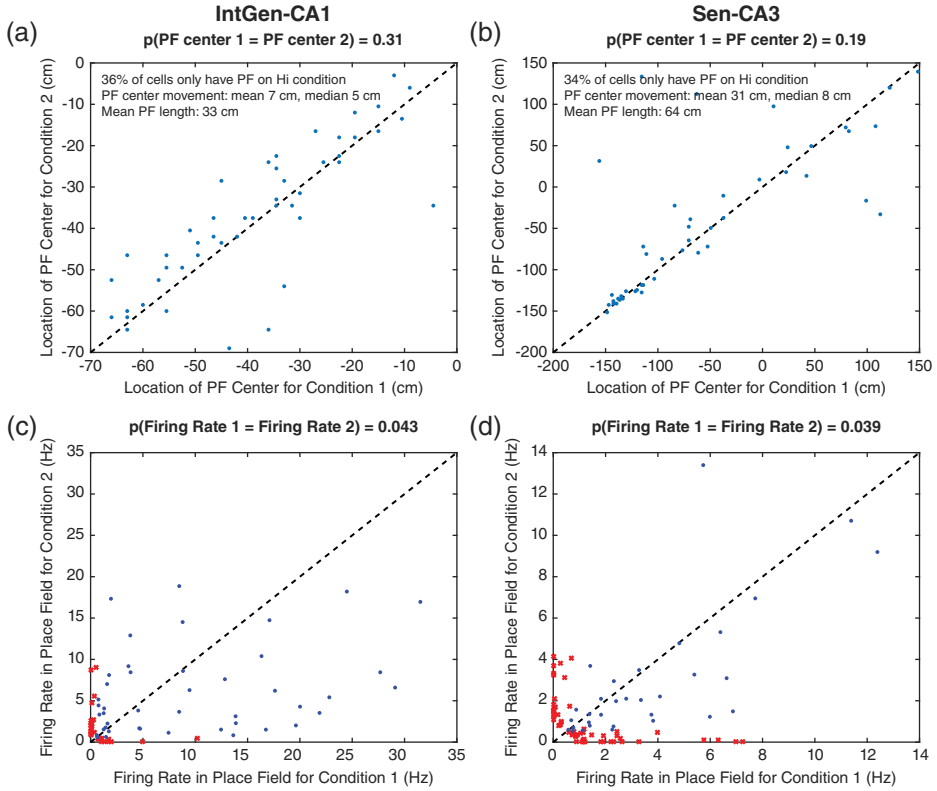

FIGURE 1 Rate remapping verification. (a,b) Each dot represents a cell, where its *x*-position is the center of the place field with maximal firing rate for condition 1, and its *y*-position is the center of the place field with maximal firing rate for condition 2. These dots fall near the dotted unity line, indicating that the locations of place fields are similar for both conditions. (a) Cells from the CA1 dataset. Condition 1 was when the animal was on the central arm coming from the left arm and going to the right arm, whereas condition 2 was when the animal was on the central arm coming from the right arm and going to the left arm. (b) Cells from the CA3 dataset. Condition 1 was the black track, and condition 2 was the white track. (c,d) Each dot represents a place field, where its *x*-position is the firing rate for condition 1 and its *y*-position is the firing rate for condition 2. These dots do not fall near the dotted unity line, indicating that firing rates for the two conditions are different. Blue dots indicate place fields with sufficient firing for both conditions to be included for subsequent analyses, whereas red *x*'s indicate place fields that were not considered rate remappers. Panel (c) shows cells from the CA1 dataset, and panel (d) shows cells from the CA3 dataset; condition definitions as in panels (a,b) [Color figure can be viewed at wileyonlinelibrary.com]

Bursts were defined as spikes with interspike intervals <10 ms (Royer et al., 2012).

Overdispersion was calculated as described in (Fenton & Muller, 1998). In short, the observed number of spikes S on a given pass through the place field is compared to the expected number of spikes $N = \Sigma R_i \Delta t$ calculated by multiplying the average firing rate at each location with the amount of time spent at that location. If there are more than four spikes expected, the Poisson distribution can be approximated by a normal distribution giving the z score $Z = \frac{S-N}{\sqrt{N}}$, which is subject to a correction of decreasing the absolute value of Z by 1/2 for transforming the discrete spike counts into a continuous z score. Passes for which fewer than four spikes were expected because of too little time spent in the place field were excluded, as in (Fenton & Muller, 1998).

All analyses were implemented in Matlab.

2.4 | Phase precession analyses

All quantifications of phase precession used the cl_corr function in the measure_phaseprec toolbox, which was provided by Richard Kempter (Kempter, Leibold, Buzsáki, Diba, & Schmidt, 2012). This toolbox itself relies on the circStat toolbox by Philipp Berens (Berens, 2009), available at http://www.mathworks.com/matlabcentral/fileexchange/10676.

Resultant length vectors in Figure 6 were calculated using the circ_mean and circ_r functions in the circStat toolbox. The circular–linear correlations in Figure 6a,d were calculated with the circ_corrcl function in the circStat toolbox. It is important to note that the circStat circ_corrcl calculates the correlation between a circular independent variable and a linear dependent variable, whereas the cl_corr function from the measure phaseprec toolbox calculates the correlation between a linear independent variable and a circular dependent variable.

3 | RESULTS

To better understand how the rate changes in response to nonspatial variables of rate remapping are expressed on short time scales, we analyzed two datasets collected from the hippocampus as rats ran on 1D tracks. Single-unit responses were recorded using standard tetrode methods; see Section 2 and (Ji & Wilson, 2008; Mankin et al., 2015) for more detail.

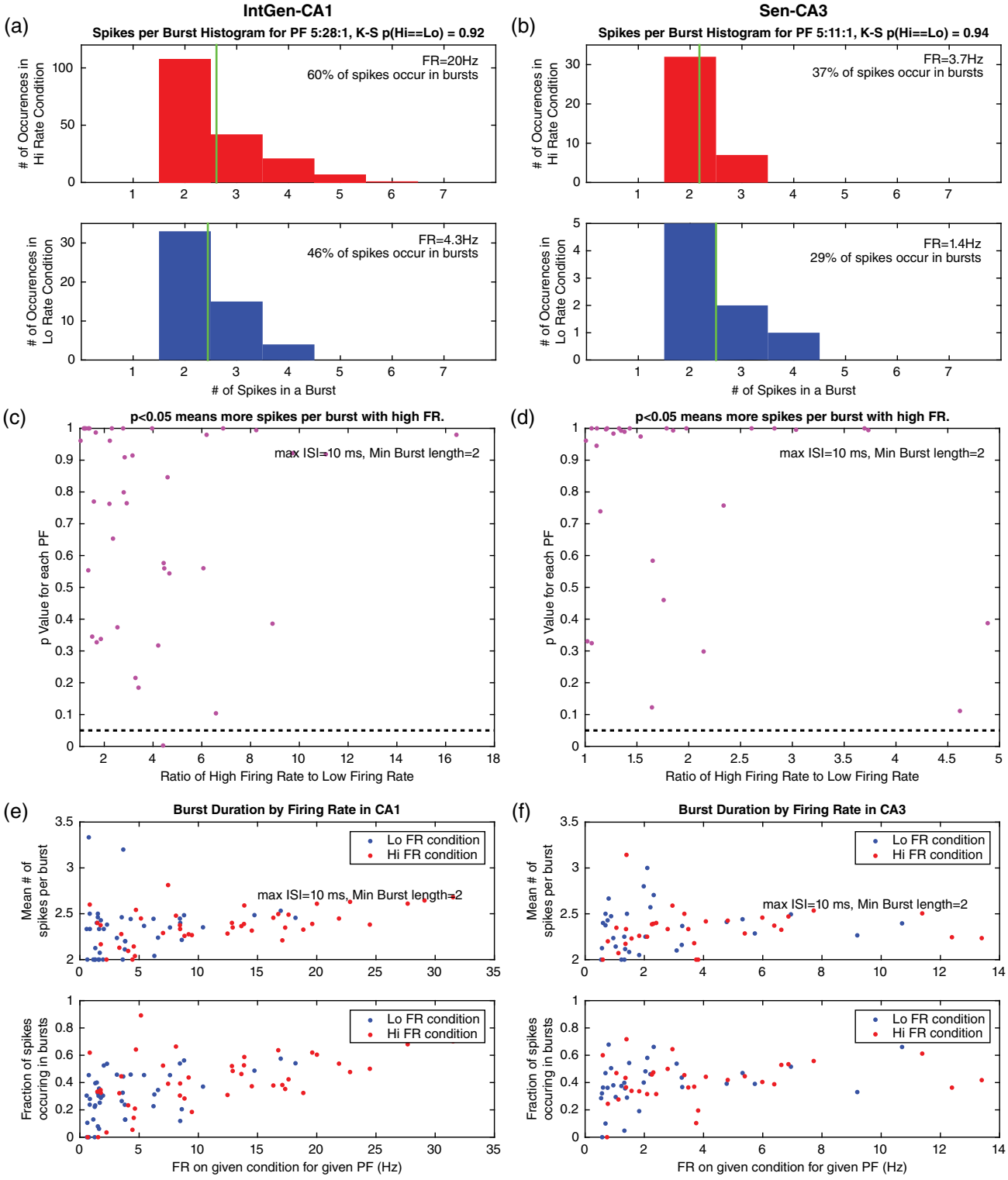

FIGURE 2 Burst duration. (a,b) Histograms of number of spikes per burst for two example place fields. Top: high rate condition, bottom: low rate condition. Mean number of spikes per burst (green lines). No significant difference between the spikes per burst distributions across conditions for either place field. Panel (a) shows data from a place field from the CA1 dataset and panel (b) shows data from a place field from the CA3 dataset. (c,d) For each place field, the distributions of spikes per burst are compared between the two conditions using the Kolmogorov–Smirnov test. The *p* value for each place field is plotted as a function of extent of rate remapping for that place field (purple dots). Very few place fields have significantly different burst length in the two conditions (dotted line at $p = .05$). Panel (c) shows place fields from the CA1 dataset and panel (d) shows place fields from the CA3 dataset. (e–f) For each place field, two dots are plotted: one (red) corresponding to the high firing rate condition and one (blue) corresponding to the low firing rate condition. On the *x* axis is the firing rate of the place field on that condition and on the *y* axis is the mean number of spikes per burst (top) or the fraction of spikes that occur in bursts (bottom). Neither of these is strongly affected by firing rate. Panel (e) shows place fields from the CA1 dataset, and panel (f) shows place fields from the CA3 dataset

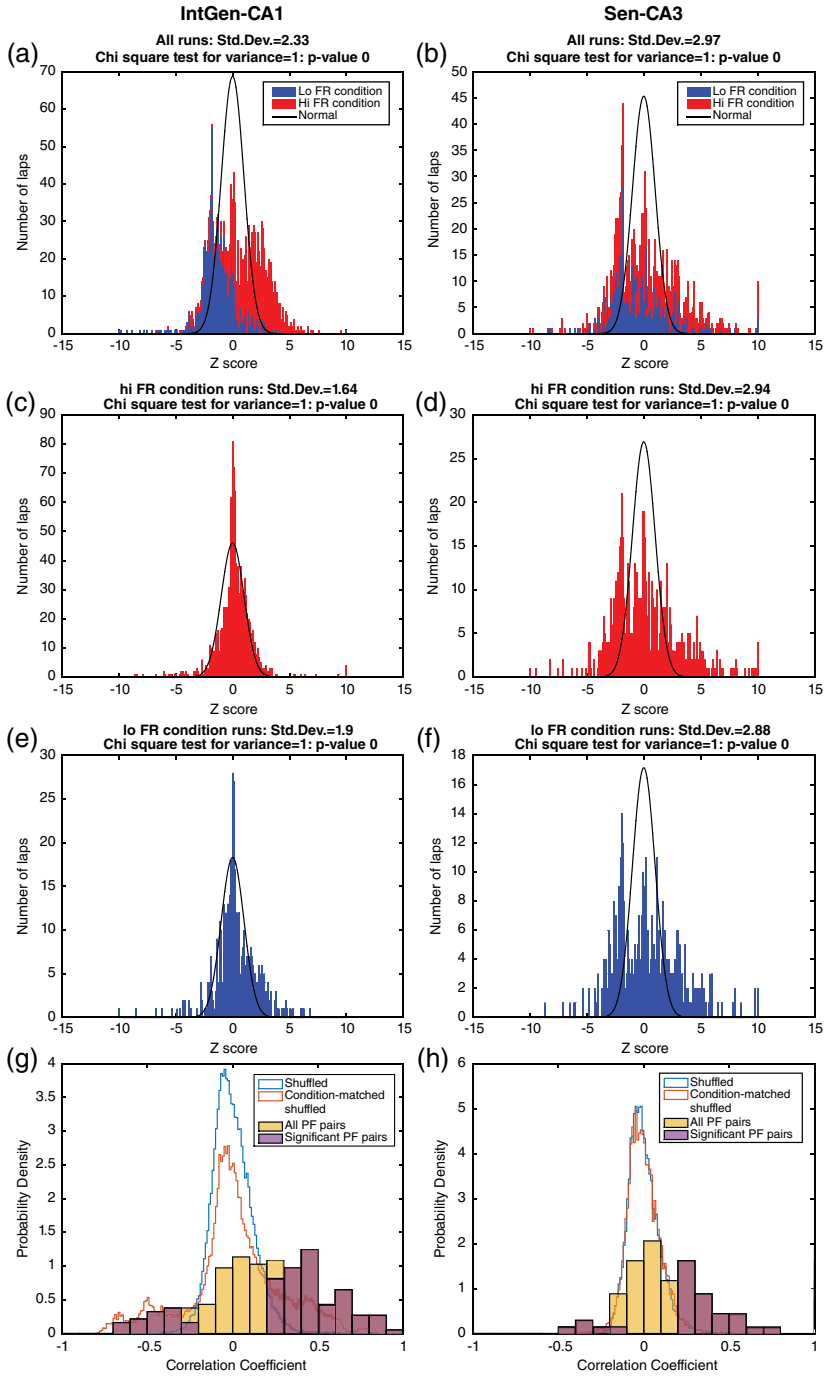

FIGURE 3 Overdispersion. (a,b) Overdispersion of all trials for all place fields. For each trial, a *z* score is calculated based on a comparison of the number of spikes expected on each trial based on the average firing rate over all trials with the number of spikes observed normalized by the expected variance. Stacked histograms are plotted where red represents trials that occurred for the high rate condition for each place field and blue represents trials that occurred for the low rate condition for each place field. The solid line shows the distribution expected if spike counts were simply Poisson (approximated by the normal distribution for sufficiently large expected spike counts; see Section 2). The histograms are highly overdispersed and show some bimodality. Panel (a) shows place fields from the CA1 dataset, and panel (b) shows place fields from the CA3 dataset. (c,d) Overdispersion for all place fields for their high rate condition. In this panel, the *z* score is calculated with respect to the average firing rate only from the high rate condition. Spike counts are still overdispersed but now seem to be more unimodal. Panel (c) shows place fields from the CA1 dataset and panel (d) shows place fields from the CA3 dataset. (e,f) Overdispersion for all place fields for their low rate condition. In this panel, the *z* score is calculated with respect to the average firing rate only from the low rate condition. Spike counts are still overdispersed, but now seem to be more unimodal. Panel (e) shows place fields from the CA1 dataset, and panel F shows place fields from the CA3 dataset. (g,h) Trial-by-trial correlations between spike counts occurring in pairs of simultaneously recorded place fields. The wide bars show the observed distribution of correlations. Place field pairs whose spike count correlations were significant are shown in purple. The null distribution achieved by shuffling trial indices independently for each place field is shown in blue. The null distribution achieved by shuffling trial indices independently for each place field, while requiring that the shuffling only be within trials with the same condition, is shown in orange. Panel (g) shows correlations from the CA1 dataset, and panel (h) shows correlations from the CA3 dataset

For the Sensory/CA3 task, recordings were obtained from CA3 with the goal of understanding the encoding of sensory information. Rats were trained to run back and forth on a 1.48 m long track to receive reward at each end of the track. Three animals were recorded on 2 days each. Each recording day consisted of four 10 min long sessions. During the first and last session, animals performed the task on the familiar black track. During the middle two sessions, the surface of the track was switched out for a novel white surface. We compared single-unit responses between trials with the black track and the trials with the white track.

For the Internal/CA1 task, recordings were obtained from CA1 with the goal of understanding the encoding of nonsensory internal state information. Rats were trained to run on a figure-8 track such that each time they ran down the central arm, they were rewarded for turning the opposite direction of the previous trial. The behavior thus requires internal generation of a marker of task condition. Recordings occurred after animals reached a performance criterion of 80% correct trials.

3.1 | Representation of nonspatial information in firing rate without affecting spatial response properties

Rate remapping is defined as changes in firing rate of place cells without changes in their spatial response. We asked whether the data collected in our tasks contains bona-fide representation of nonspatial information by modulation of place cell firing rates as opposed to statistical noise or misdiagnosis of changes in spatial response properties, as might be observed in global remapping (Colgin, Moser, & Moser, 2008; Muller, Kubie, & Ranck, 1987). In this and all following analyses, we separated each pass through the place field into one of two conditions: black track or white track for the Sensory/CA3 data, and going from left to right or going from right to left for the Internal/CA1 data. For the Sensory/CA3 data, we treated the activity of each cell occurring on rightward passes and leftward passes independently, as we found independence of place cell activity for opposite directions of motion (data not shown, see also Markus et al., 1995).

First, we calculated place field locations for each condition independently according to criteria described in Section 2. We calculated the center of the place field with maximal firing rate for each cell under each condition, and found no significant difference between place field locations for each cell under the two conditions (Figure 1a, b); $p > .05$, paired $t_{CA1} = -1.0$, $df_{CA1} = 46$, 95% confidence interval of mean difference [−4.5 1.5]; paired $t_{CA3} = -1.3$, $df_{CA3} = 45$, 95% confidence interval of mean difference [−31 6.5]; mean and median movement < mean place field size, see Figure 1a,b for values). For all following analyses, we calculated place field locations using activity during both conditions, and compared activity in those place fields across conditions.

After verifying that the locations of place fields were largely consistent across the conditions, we compared the firing rates within each place field across the conditions. Average firing rates in each place field were significantly different between the two conditions (Figure 1c,d; paired t test $p < .05$; $t_{CA1} = 2.1$, $df_{CA1} = 74$, $t_{CA3} = 2.1$, $df_{CA3} = 86$). In particular, 66% of Internal/CA1 place fields and 34% of Sensory/CA3 place fields had significantly different ($p < .01$, 2 sample Kolmogorov–Smirnov test) trial-by-trial spike counts between the two conditions.

Both of these analyses (Figure 1) demonstrate a heterogeneity within the population. One group of place cells completely change their place fields in response to the condition change, reminiscent of global remapping. However, these results also demonstrate a subpopulation of place cells that retain their spatial response properties while simultaneously changing their firing rates in response to the condition change, conforming to the definition of rate remapping. Such a heterogeneous response to a manipulation has observed previously (Muller & Kubie, 1987) and is referred to as partial remapping (Colgin et al., 2008). We will focus in this paper on the population of rate remappers.

For the CA1 data, of 198 units recorded, 74 had place fields on the central track. One cell had two place fields on the central track for a total of 75 place fields (all dots in Figure 1c). Of those, 44 place fields had firing for both conditions (green dots in Figure 1c), and were included for subsequent analyses. For the CA3 data, of 154 units recorded, 37 had place fields on leftward passes and 33 had place fields on rightward passes. Of those, 17 cells had multiple place fields for a total of 87 place fields (all dots in Figure 1d). Of those, 32 place fields had firing for both conditions (green dots in Figure 1d), and were included for subsequent analyses. For additional information on criteria for inclusion and relevant definitions, see Section 2. Subsequent analyses will compare between the "high-rate condition" and the "low-rate condition". The identities of these conditions are defined on a place field-by-place field basis: the "high-rate condition" is the condition for which that particular cell has a higher firing rate in that place field. Thus, the same condition (e.g., black track for the Sensory/CA3 data) may be the high-rate condition for one place field and the low-rate condition for another.

3.2 | Burst coding

What is the fine-scale temporal structure of these rate changes? It has been suggested (Kepecs & Lisman, 2003) that information could be coded in the duration (number of spikes) of the high-frequency bursts that are known to be emitted by hippocampal place cells (Ranck, 1973); bursts including a variable number of spikes would allow for graded changes in firing rate. To explore this possibility, we produced histograms of the number of spikes occurring in each burst in the place field under each condition. We defined a burst as spikes with inter-spike intervals of less than 10 ms (Royer et al., 2012). The histograms for two example place fields are shown in Figure 2a,b. Population data is shown in Figure 2c,d. Most place fields do not have significantly more spikes per burst for their high rate condition than for their low rate condition. Number of spikes per burst and fraction of spikes that occur in bursts only weakly increase as a function of firing rate (Figure 2e,f). These findings are consistent for both datasets. We calculated the contribution of changes in burst duration to changes in firing rate across conditions by plotting the fold change in firing rate against fold change in burst duration for each place field. The slope of the best fit line was calculated subject to the constraint that it pass through (1, 1), corresponding to a hypothetical place field with no change in firing rate and no change in burst duration. That

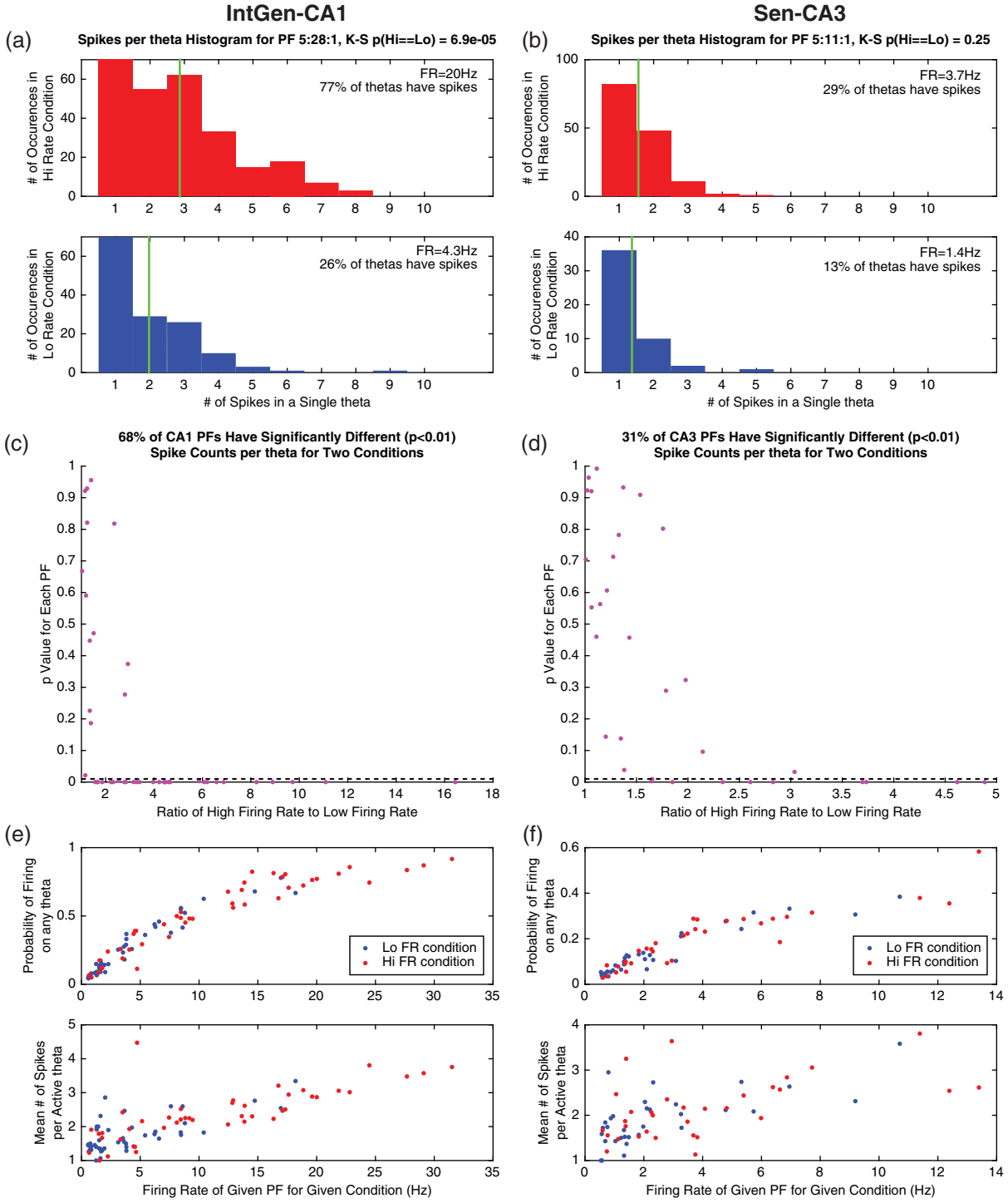

FIGURE 4 Theta cycle spiking statistics. (a,b) Histograms of number spikes per theta cycle for same example place fields as Figure 2a,b. Only theta cycles in which there was at least one spike (where the appropriate map is being used, so stereotyped activity is expected) are counted. Top: high rate condition; bottom: low rate condition. Mean number of spikes per active theta cycle (green lines) is different in the two conditions. Panel (a) shows data from a place field from the CA1 dataset and panel (b) shows data from a place field from the CA3 dataset. (c,d) For each place field, the distributions of spikes per theta cycle are compared between the two conditions using the Kolmogorov–Smirnov test. The *p* value for each place field is plotted as a function of extent of rate remapping for that place field (purple dots). Almost all place fields with greater than twofold rate remapping had highly significant increases (dotted line at $p = .01$) in number of spikes per theta cycle, even when limited to theta cycles for which there was at least one spike in the place field. Panel (c) shows place fields from the CA1 dataset, and panel (d) shows place fields from the CA3 dataset. (e,f) For each place field, two dots are plotted: one (red) corresponding to the high firing rate condition and one (blue) corresponding to the low firing rate condition. On the *x* axis is the firing rate in the place field for that condition, and on the *y* axis is the probability of firing in any theta cycle for which the animal is in the place field (top) or the mean number of spikes that occur in a theta cycle, when restricted to theta cycles for which there was at least one spike (bottom). Panel (e) shows place fields from the CA1 dataset, and panel (f) shows place fields from the CA3 dataset

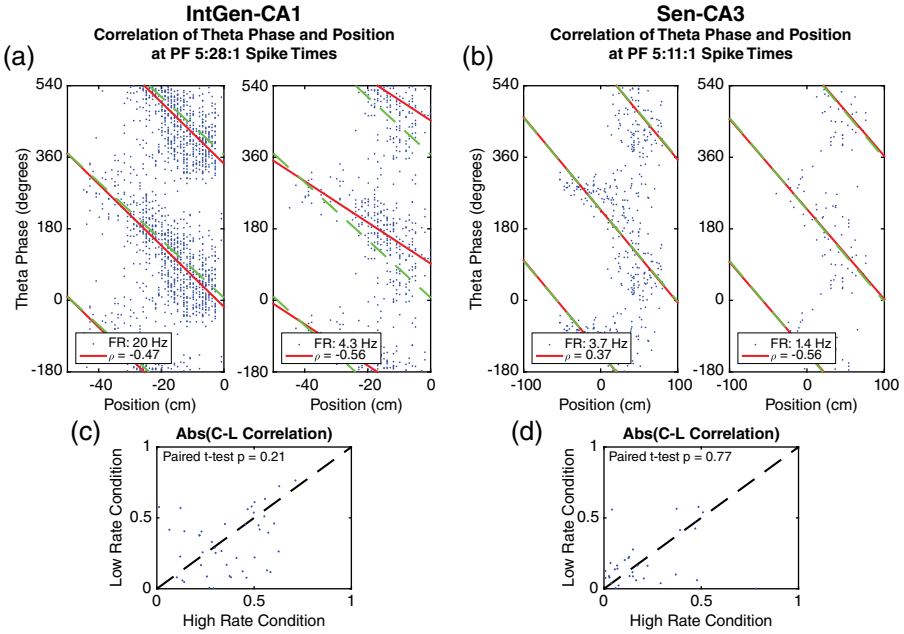

FIGURE 5 Phase precession quality. (a,b) Classic plot of phase precession for same example place fields as Figures 2A,B and 4A,B. Each dot represents a spike, where the *x* position corresponds to the position of the animal at the time that spike was fired, and the *y* position corresponds to the theta phase at the time of the spike. In this plot, phase precession is observed as a negative correlation between position and phase. Best fit lines are shown, calculated using only spikes fired for that condition (red line) or using spikes from both conditions (green dashed line). The magnitudes of the circular linear correlation (Kempter et al., 2012) values are very similar for both conditions, suggesting that the quality of phase precession is the same despite the several-fold change in firing rate. Panel (a) shows phase precession of a place field from the CA1 dataset, and panel (b) shows phase precession of a place field from the CA3 dataset. (c,d) Each dot represents the phase precession quality of a place field, where its *x* position is the absolute value of the circular–linear correlation coefficient for the high firing rate condition and its *y* position is the absolute value of the circular–linear correlation coefficient for the low firing rate condition [Color figure can be viewed at wileyonlinelibrary.com]

slope represents the fraction of the observed rate change across conditions attributable to the observed changes in burst duration. In the Sensory/CA3 data, changes in burst duration contributed .54% of the rate changes across condition. In the Internal/CA1 data, changes in burst duration contributed .25% of the rate changes across condition. These data lead to the conclusion that rate remapping is not the result of modulation of number of spikes per burst.

3.3 | Excess variability in place cell spiking: Overdispersion

We next turned to analysis of trial-to-trial variability in spatial response properties of place cells, termed "overdispersion" (Fenton & Muller, 1998). The observation is that the number of spikes that occur on a given pass is more variable than would be expected from a Poisson process with a constant rate. Single-pass spike count *z* scores are calculated by comparing the number of spikes actually observed to the number of spikes expected on that pass given the length of time the animal spent at each location multiplied by the long-term average firing rate at each location. Histograms of these *z* scores are considered to be overdispersed if they are broader than the normal distribution, which reasonably approximates the Poisson distribution under certain assumptions described in Section 2. A perfect Poisson process would produce *z* scores with a standard deviation of 1. Biologically relevant processes such theta phase and refractory history introduce enough violation of Poisson process assumptions to cause the lowest biologically feasible values of overdispersion to be larger than 1 (Barbieri, Quirk, Frank, Wilson, & Brown, 2001). In general, larger overdispersion values imply that there are other variables affecting spike counts beyond the variables already taken into account. In our data, we found that spike counts were strongly overdispersed. This overdispersion can be seen by the deviation of the spike count histograms from the normal distribution of *z* scores (black curve) that would be expected if firing were Poisson (Figure 3a,b). The extent of overdispersion, as quantified by the *z* score of single trial spike counts, was decreased by separating out the high rate condition from the low rate condition in both datasets (Figure 3c,f). The Internal/CA1 data had two peaks of spike count *z* scores (Figure 3a), one peak at +3SD and one peak at −3SD) that were cleanly separated by condition (Figure 3c,e). This separation of single trial spike counts by condition decreased overdispersion from 2.33 over all trials to 1.64–1.90 for a single trial type. Overdispersion was not decreased for the Sensory/CA3 data by splitting trial types: overdispersion was 2.97 over all trials and 2.88–2.94 for a single trial type. It is possible that the decrease in overdispersion specific to the CA1 data was a result of the greater proportion of place fields with significant rate remapping observed in the Internal/CA1 data.

Is this variability in firing a single-cell phenomenon, or is it reflective of coordinated trial-to-trial changes across the population? We looked at correlation of single-trial spike counts occurring in pairs of simultaneously recorded place fields (filled bars in Figure 3g,h) comparing spike counts in place field A with spike counts in place field B on the same trial. In order to test whether the observed spike counts were more correlated on the whole than expected by chance, we

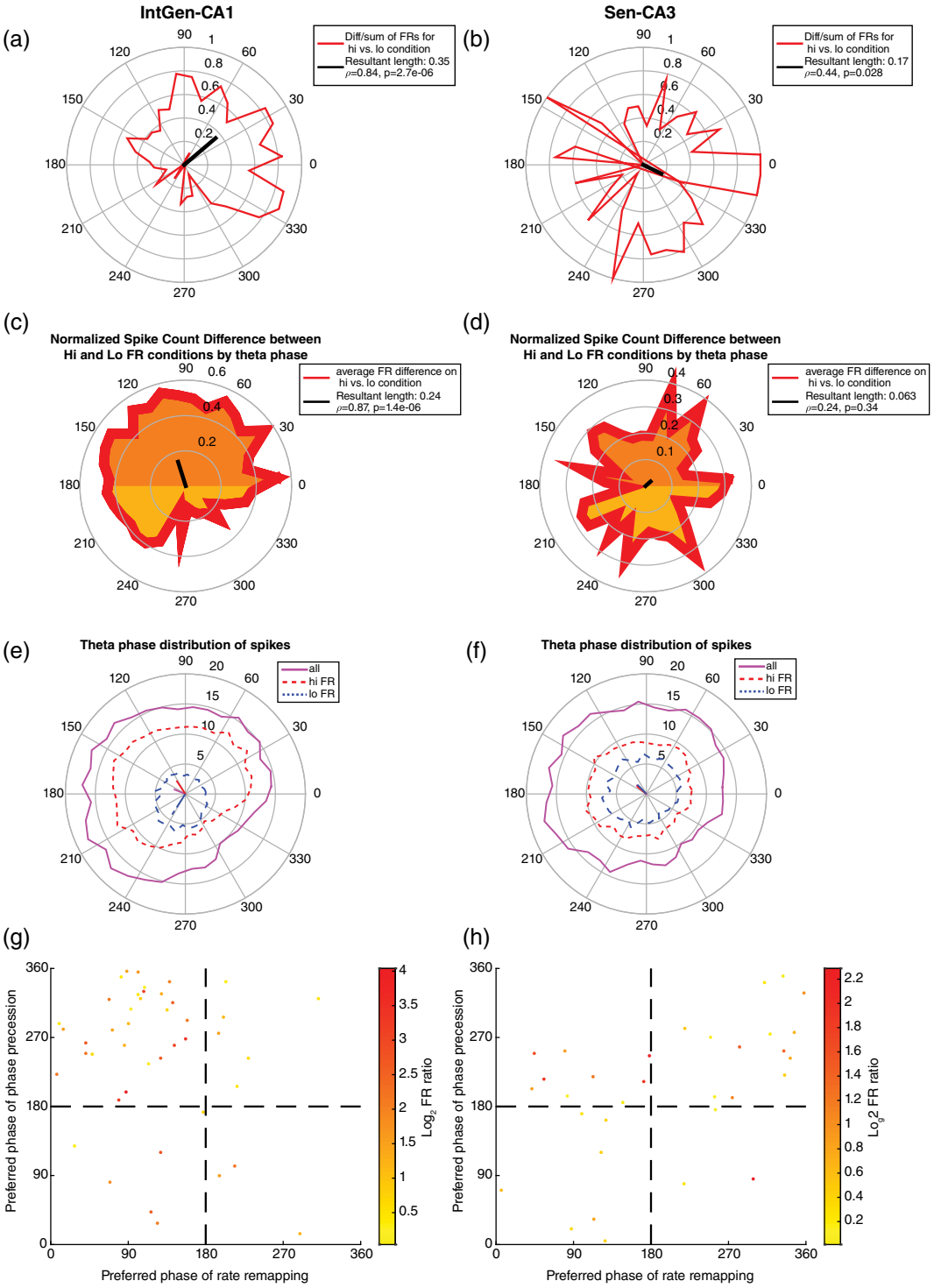

FIGURE 6 Two halves of theta contain different phenomena. (a,b): Rate remapping extent by theta phase for same example place fields as Figures 2a,b, 4a,b and 5a,b. In red is shown the normalized spike count difference between the high and low firing rate (FR) conditions for each theta phase bin. Panel (a) shows a place field from the CA1 dataset, and panel (b) shows a place field from the CA3 dataset. (c,d) The red line shows the population-wide average of the firing differences shown in panels (a and b). The average normalized difference for the CA1 dataset (c) ranges from ~.2 at ~270° to ~.5 at ~90°. The firing rate difference is heavily weighted towards the first half of theta, as quantified by the resultant vector, which is plotted on an *r* axis with a range of [0, 1]. The CA3 data (d) did not show a significant bias. (e,f) Theta phase histogram of spikes in the low and high rate conditions. For the CA1 dataset (e), theta phase preference shifts from second half of theta to first half of theta between low and high rate conditions, demonstrating a suppression of first half firing during the low rate condition in addition to the increase in first half firing for the high rate condition. For the CA3 dataset (f), no significant effect exists. (g,h) For each place field, the preferred phase of rate remapping is plotted on the *x* axis, and the preferred phase of phase precession is plotted on the *y* axis. (g) Phase preferences of place fields from the CA1 dataset. Place fields cluster in the top left corner corresponding to a preference of rate remapping for the first half of theta and a preference of phase precession for the second half of theta. (h) Phase preferences of place fields from the CA3 dataset. Place fields are over-represented in the top half, corresponding to a preference of phase precession for the second half of theta, but there does not seem to be a consistently preferred phase of rate remapping [Color figure can be viewed at wileyonlinelibrary.com]

generated two null distributions. One (blue line in Figure 3g,h: "shuffled") was generated by calculating spike count correlations between place field A from some trial and place field B on another random trial. The second distribution (orange line in Figure 3g,h: "condition-matched shuffled") was generated by calculating spike count correlations between place field A from some trial and place field B on a random trial from the same condition. For both datasets, the empirical distribution has more extreme values than the condition-matched shuffled distribution, which in turn had more extreme values than the shuffled distribution. The extent of extremity differed between the datasets however. The Kolmogorov–Smirnov distance statistic D roughly corresponds to the fraction of place field pairs with more extreme values. For the Internal/CA1 dataset, distance was $D_{37000,37000} = .15$ between the shuffled and condition-matched shuffled distributions, and distance was $D_{37000,185} = .33$ between the condition-matched shuffled and observed distributions. For the Sensory/CA3 dataset, distance was $D_{13600,13600} = .02$ between the shuffled and condition-matched shuffled distributions, and distance was $D_{13600,68} = .38$ between the condition-matched shuffled and observed distributions. For both datasets, spike count correlations were higher on a trial-by-trial basis than would be expected by simply controlling for condition. Thus, there is at least some population-level coordination of variability.

3.4 | Rate modulation as changes in probability of discrete states?

As noted in the introduction, there are two ways to achieve a change in firing rate. One is that the nonspatial variable modulates the firing rate of a place cell in its place field, and spike counts at any particular time are drawn from a Poisson distribution with that characteristic rate. Another option ("discrete state probability" hypothesis) is that the nonspatial information can affect the probability of the expression of an all-or-none firing phenomenon. For example, imagine that the network has two states, one in which the place field exists, and one in which it does not. Changes in probability of that place field existing would show up as continuous changes in long-term average firing rate even if there are discrete underlying states (place field existing or not existing). State transitions have been hypothesized to occur in the hippocampus with the theta cycle being the smallest unit of time over which states are considered stable (Jackson & Redish, 2007; Jezek et al., 2011). We looked at all theta cycles (the smallest unit of time hypothesized to contain a single state) that the animal was in a particular place field, and divided the data between theta cycles in which the cell fired and theta cycles in which it did not. One can calculate the fraction of theta cycles that the animal was in the place field for which the cell was active (text insets of Figure 4a,b and top panels of Figure 4e,f). The probability of being active in a given theta cycle does increase with increasing firing rate, a result consistent with both hypotheses. The discrete state probability hypothesis makes the additional prediction that if analysis is restricted to times when the network is in a given state, firing behavior should be consistent. Therefore, if we only look at theta cycles for which the cell is active in its place field (i.e., theta cycles when the network is in the state for which the place field exists), the spike count distribution (Figure 4a,b) should be the same no matter the rate remapping condition. However, the number of spikes per theta cycle increases in the high firing rate condition, even when restricting analysis to active theta cycles (when the network state presumably corresponds to the one in which the place field exists; Figure 4a,d, bottom panels of Figure 4e,f). Therefore, we do not find evidence of discrete states in which the place field either does or does not exist.

3.5 | Coexistence of rate remapping and phase precession

The question of how rate changes involved in rate remapping interact with fine-scale temporal patterning of place cell firing remains unanswered. Place cells express a phenomenon known as "phase precession" (Jensen & Lisman, 1996; O'Keefe & Recce, 1993; Skaggs et al., 1996), which is the observation of a negative correlation between position of the animal and theta phase of a cell's spikes. It seems possible that increased spiking under the high rate condition may degrade the theta phase code. The question then arises, is the quality of phase precession affected by rate remapping? We compared the quality of phase precession between the high and low rate conditions for each place field. We used the absolute value of the circular–linear correlation coefficient developed by (Kempter et al., 2012), as the sign of the circular–linear correlation coefficient does not always match up with the sign of the best fit slope (Kempter et al., 2012) (Figure 5). We did not find a significant difference in phase precession quality between the conditions in either data set ($p > .05$, paired $t_{CA1} = 1.3$, $df_{CA1} = 43$, paired $t_{CA3} = .3$, $df_{CA3} = 31$).

3.6 | Specialization of two halves of theta

Previous work has suggested different functions of the two halves of the theta cycle (Hasselmo et al., 2002; Sanders et al., 2015), where the first half of theta is for current experience (encoding) and the second half for upcoming predictions (retrieval). We use the convention that the peak of theta at the local pyramidal cell layer is 0°. For each place field, we constructed a polar histogram of spikes occurring in the place field binned by theta phase under each condition. We then took the difference of spike counts in each theta phase bin between the two conditions divided by the sum of the spike counts in that phase bin to get a normalized difference in firing between the conditions at each theta phase (Figure 6a,b); theta phase bins with more firing on the low firing rate condition have a negative normalized difference, therefore their values are reflected across the origin in the polar plot). At each phase bin, we averaged the normalized firing difference across all place fields, giving an average firing difference between the high and low rate conditions by theta phase for the entire population (Figure 6c,d). For the Internal/CA1 data, the firing difference is large during the first half of theta and smaller during the second half of theta. Circular statistics give the mean resultant vector, whose direction signifies the theta phase preference of rate remapping and whose magnitude signifies the strength of that preference. Rate remapping in the Internal/CA1 data had a preferred phase of 90° and a resultant length of .24 (Figure 6c; circular–linear correlation $\rho = .87$, $p < .01$, $df = 34$). We plotted a theta phase histogram of all spikes occurring on the low and high rate conditions (Figure 6i). The theta phase preference clearly shifts from the

second half of theta for the low rate condition to the first half of theta for the high rate condition, demonstrating that firing is increased for the high rate condition during the first half of theta and is actually suppressed for the low rate condition during the first half of theta. The Sensory/CA3 data did not show significant theta phase dependence of rate remapping (Figure 6d; resultant length .06, circular–linear correlation $\rho = .24$, $p > .05$, $df = 34$).

The strong expression of rate remapping during the first half of theta observed in our Internal/CA1 data complements previous work that has shown a preferential expression of phase precession during the second half of theta (Mehta, Lee, & Wilson, 2002; Yamaguchi, Aota, McNaughton, & Lipa, 2002). We verified this with a novel analysis parallel to the rate remapping analysis above. The magnitude of the circular–linear correlation of phase precession (Kempter et al., 2012) was calculated for a sliding 90° window every 10°, generating a polar plot analogous to those shown in Figure 6a,b, where the radial value is phase precession quality instead of rate remapping magnitude. The mean resultant vector was calculated for the phase precession quality polar plot of each place field (not shown). For each place field, we plotted the direction of that mean resultant vector for phase precession on the *y* axis and the direction of the mean resultant vector of rate remapping on the *x* axis (Figure 6g,h). Place fields in the Internal/CA1 dataset clustered in the top left corner corresponding to a preference of rate remapping for the first half of theta and a preference of phase precession for the second half of theta. This analysis demonstrates a separation of rate remapping and phase precession into separate halves of the theta cycle; see below for discussion of difficulties in interpreting the Sensory/CA3 data (end of "Two halves of theta dedicated to rate remapping and phase precession respectively" in the Section 4).

4 | DISCUSSION

For place cells of the hippocampus, spatial relation can be expressed through the fine-scale temporal ordering of firing that occurs during the theta sequences associated with phase precession (Foster & Wilson, 2007; Jensen & Lisman, 1996; Lisman & Redish, 2009; O'Keefe & Recce, 1993; Skaggs et al., 1996). Place cells can also represent nonspatial information in their firing rates (Aronov, Nevers, & Tank, 2017; Leutgeb et al., 2005; Wood et al., 2000). In this study, we looked at the fine-scale temporal behavior of firing rate changes of place cells in response to nonspatial changes.

4.1 | Co-existence of independent rate and temporal codes

Whether neurons use rate codes or temporal codes to represent information has been a source of controversy (Brette, 2015; Gautrais & Thorpe, 1998; Shadlen & Newsome, 1994; Softky, 1995). Here, we demonstrate that two independent information streams can be simultaneously represented in a single spike train. Several-fold firing rate changes in response to nonspatial information can occur in place cells without degrading the quality of the theta phase coding of location within the place field. Previous work had suggested that place cells had such an ability to represent independent information content in theta phase and firing rate, specifically in the case of the rate changes due to changes in running speed (Huxter, Burgess, & O'Keefe, 2003; O'Keefe & Burgess, 2005). However, the firing rate changes associated with running speed are hard to disentangle from the natural relationship between velocity and position (Terrazas et al., 2005), so it was not clear whether rate changes due to running speed would apply to other types of rate changes. We now extend more recent reports of the independence of rate remapping and phase precession (Allen et al., 2012) in showing the general applicability of this independence of rate and temporal coding.

4.2 | Phase precession: Models and analysis

The question of the origin of phase precession has alternatively been suggested to be generated as a network process or as a single-cell phenomenon, reviewed in (Maurer & McNaughton, 2007). In particular, it had been suggested that the excitation received by a place cell slowly ramped up over the length of the place field. When combined with oscillatory inhibition, spiking would occur progressively earlier in the theta cycle as excitation ramped up, leading to the observation of phase precession (Harvey, Collman, Dombeck, & Tank, 2009; Kamondi, Acsády, Wang, & Buzsáki, 1998; Lengyel, Szatmary, & Erdi, 2003; Mehta et al., 2002). However, the results of the current study contradict such a model. We see that phase precession and the extent of excitation are independent phenomena, as the quality of phase precession is maintained over several-fold changes in firing rate. This is in addition to other recent evidence of dissociation of place fields from phase precession (Aghajan et al., 2014; Feng et al., 2015; Schlesiger et al., 2015). Current thought assigns generation of phase precession to the grid cells of the entorhinal cortex (Barry, Ginzberg, O'Keefe, & Burgess, 2012; Erdem & Hasselmo, 2012; Jaramillo, Schmidt, & Kempter, 2014; Kubie & Fenton, 2012; Sanders et al., 2015), although experience-driven learning (likely occurring in the hippocampus itself) transforms phase precession to full-blown theta sequences (Feng et al., 2015).

Single-cell models of phase precession were supported by the observation that phase precession plots where position was replaced on the *x* axis with instantaneous firing rate still generate the negative correlation representative of phase precession (Harris et al., 2002), but see (Huxter et al., 2003). However, our work demonstrates that a strong confound in such an analysis is that changes from low rate condition to high rate condition during rate remapping change the theta phase preference of firing due to suppression of firing during the first half of theta under the low rate condition. This effect leads to an artificially strong correlation between instantaneous firing rate and theta phase of firing. While this analysis technique has the benefit of being a "quick and dirty" method for quantifying phase precession, analysts should be aware of the confound of nonspatial information in the relationship between firing rate and theta phase of firing.

4.3 | Burst coding

It has been suggested that burst duration might encode information (Kepecs & Lisman, 2003), and indeed burst duration coding is present in other neural systems (Avila-Akerberg, Krahe, & Chacron, 2010). However, in this hippocampal data, the number of spikes per burst

TABLE 1 Spatial and temporal segregation of CA1 phenomena

Phenomenon	Theta phase preference of phenomenon	Input necessary for that phenomenon	CA1 layer receiving that input	Gamma frequency of that CA1 layer	Theta phase of that γ band and CA1 layer
Rate remapping	~0–180° [1]	PFC via thalamus [2]	L-M (distal) [3]	~60–100 Hz [4]	~270–90° [4]
Phase precession	~180–360° [1]	Medial EC2 via CA3 [5]	Radiatum (proximal) [6]	~30–60 Hz [4]	~90–200° [4]

For each firing phenomenon expressed by CA1 place cells, this table shows the theta phase during which that phenomenon is dominant, the input giving rise to that phenomenon, and which layer of CA1 that input arrives in.
EC2, layer II of entorhinal cortex; L-M, lacunosum-moleculare; PFC, prefrontal cortex. [1]: Current paper, [2]: Ito et al. (2015), [3]: Ramón y Cajal (1911), [4]: Schomburg et al. (2014), [5]: Schlesiger et al. (2015), Jaramillo et al. (2014), [6]: Herkenham (1978), Steward and Scoville (1976).

does not seem to change as a function of rate remapping condition. It should be noted that spike shape changes as bursts progress, so it is possible that biases in spike clustering may have truncated bursts. The fraction of spikes occurring in bursts did change, but not enough to account for the observed rate changes. Thus, burst parameters do not explain the representation of nonspatial information in rate remapping.

4.4 | Multiple maps hypothesis and population coordination of activity

The relationship between single cell rate remapping and population-level representation is not simply summarized. On the one hand, there is clearly correlated variability (sometimes referred to as "noise correlations"; Miura, Mainen, & Uchida, 2012) among the place cell population during rate remapping, even after taking into account the externally observable variables that the place cells are responding to (Figure 3g,h). This result implies that there are intrinsic population dynamics that coordinate place cell activity. However, the activity of individual place cells does not seem to be constrained to discrete network states. There is rather large heterogeneity of place cell behaviors: some place cells "globally remap" (i.e., gain or lose place fields at given locations) while other place cells "rate remap" (i.e., maintain place field location but have consistently different firing rates under the different conditions). Moreover, rate remapping is not simply a long-term average of an all-or-none firing phenomenon with a rate that depends on condition (Figure 4), as would be expected if there were multiple maps that were being switched between, one in which the cell has a place field at that location and others in which it does not (Jackson & Redish, 2007; Kelemen & Fenton, 2016; Olypher et al., 2002). Rather, we show that even when restricting analysis to theta cycles on which a cell is active and therefore in the appropriate map, there are still firing rate changes between the conditions. This result is more in line with the idea that place cells have very high-dimensional spatial/nonspatial receptive fields, for which many variables can have independent effects (Rangel, 2012; Wu, 2012). Indeed, the overdispersion of single-pass spike counts increases between CA3 and CA1 (Mankin et al., 2012), potentially corresponding to an increase in the dimensionality of the representation with progressive processing. Finally, we observe that splitting trials by condition reduces the overdispersion of spike counts thought to be a result of unaccounted for map switches. In the Internal/CA1 data, this reduction of overdispersion is so complete as to reduce overdispersion to levels expected by chance. Even so, the low-overdispersion "maps" particular to each condition involve characteristic firing rates in each condition, not characteristic place field locations. Taken together, these results indicate the need for further research into the relationship between single cell and population-level representation of nonspatial information, as that relationship is not entirely straightforward.

4.5 | Two halves of theta dedicated to rate remapping and phase precession, respectively

We have shown here that, in our Internal/CA1 data, place cells represent different types of information during the two halves of theta. Rate changes due to rate remapping preferentially occur during the first half of the theta cycle. On the other hand, the negative correlation between position and theta phase of spiking characteristic of phase precession is stronger during the second half of the theta cycle. It seems that, during the first half of the theta cycle, place cells exhibit rate remapping, and during the second half of theta, place cells exhibit phase precession.

The separation of the theta cycle into halves dedicated respectively to rate remapping and phase precession in CA1 parallels the distinct inputs that give rise to these phenomena. Anatomically, CA1 cells receive spatially segregated inputs onto their apical dendrites (reviewed in Witter, 2010). Proximally, in the stratum radiatum, CA1 cells receive input from the CA3 region of the hippocampus (Ramón y Cajal, 1911). Distally, in the stratum lacunosum-moleculare, CA1 cells receive direct input from layer III of the entorhinal cortex (EC3) as well as from the prefrontal cortex (PFC) via the nucleus reuniens of the thalamus (Herkenham, 1978; Steward & Scoville, 1976).

These two inputs as defined by anatomy seem to correspond respectively to phase precession (stratum radiatum or SR) and rate remapping (stratum lacunosum-moleculare or SL-M; see Table 1). Phase precession does not originate in CA1, as medial entorhinal cortex (MEC) lesions eliminate hippocampal phase precession without degrading place fields (Schlesiger et al., 2015). CA1 receives MEC input through two pathways: the direct path from EC3 mentioned above and an indirect path from layer II of entorhinal cortex (EC2) via the trisynaptic pathway through DG and CA3. Grid cells in EC3 do not phase precess, whereas grid cells in EC2 do (Hafting, Fyhn, Bonnevie, Moser, & Moser, 2008; Mizuseki, Sirota, Pastalkova, & Buzsáki, 2009), so phase precession in CA1 may be inherited indirectly from EC2 via the CA3 input in stratum radiatum (Jaramillo et al., 2014). In contrast, rate remapping on this task has been shown to depend on the PFC input to CA1 via nucleus reuniens of the thalamus and is not observed in CA3 (Ito et al., 2015); therefore, this information likely is received in stratum lacunosum-moleculare, where thalamic synapses occur. It is important to note that not all rate remapping information in the hippocampus arrives through this pathway. For example, sensory related

rate remapping in CA3 depends on lateral entorhinal cortex (LEC) input (Lu et al., 2013).

Each layer is associated with a gamma rhythm of a particular frequency. CA1 spiking couples with gamma frequencies stereotypical of these inputs in a function-, place-, and theta phase-specific way (Bieri et al., 2014; Colgin et al., 2009; Zheng et al., 2016), so these gamma rhythms are thought to correspond with specific computations. The strength of the inputs into these two layers (as measured by theta/gamma cross-frequency coupling in each layer) have been shown to peak during opposite halves of the theta cycle (Schomburg et al., 2014). It seems the SR-associated slow gamma is strongest near the trough of theta (Schomburg et al., 2014) and the SL-M-associated mid gamma seems to be strongest near the peak of theta (using a theta reference of the pyramidal cell layer theta) (Schomburg et al., 2014). These phase estimates require further verification as another paper using different recording and analysis methods found different preferred phases of these gamma bands (Colgin et al., 2009). The ~90° phase difference between the (Schomburg et al., 2014) theta phase preferences and our findings can potentially be explained in two ways. One is that phase precession in CA3 itself occurs following the phase of maximal firing of CA3 place cells (Mizuseki et al., 2009; Mizuseki, Royer, Diba, & Buzsaki, 2012), so we would expect phase precession in CA1 inherited from CA3 to occur following the phase of maximal CA3/SR input. The other is that it takes time for inputs to travel down the dendrite to the point of affecting somatic firing (London & Häusser, 2005), so distal inputs may be temporally shifted relative to their effect on firing. It is also important to note that the work on gamma frequency and theta phase of SL-M fits with theta phase and gamma frequency of the EC3 input that arrives in that layer (Schomburg et al., 2014). However, little is known about the theta phase or gamma frequency associated with the thalamic input to SL-M carrying prefrontal information which gives rise to the rate remapping observed in our data.

In summary, CA1 inputs corresponding to rate remapping on the alternation task and phase precession are spatially segregated on the dendrites of CA1 pyramidal cells, and their stereotypical zones alternate maximum activation during the course of the theta cycle. As CA1 rate remapping on this task occurs preferentially during the first half of theta, it is likely that its essential input, thalamic relay neurons of the nucleus reuniens, are theta modulated. The temporal and spatial segregation of inputs to CA1 is summarized in Table 1.

This separation of representations fits very nicely with a recent theoretical suggestion about a functional dichotomy between the halves of theta (Sanders et al., 2015). That proposal describes a two-step interaction between place cells and grid cells during active navigation: during the first half of theta, place cells merge diverse information streams to accurately estimate current position. During the second half of theta, grid cells use their knowledge of spatial structure to generate sequential predictions of upcoming locations ("mind-travel") and then pass this sequence on to place cells in order to recover associates of upcoming locations. This separation is potentially compatible with a separation of theta into "encoding" (current position) and "retrieval" (mind-travel) phases (Hasselmo et al., 2002), a separation that has recently been supported with theta phase-specific optogenetic simulation (Siegle & Wilson, 2014).

How does rate remapping correspond with representation of current position/encoding of experience in these theories? One might think that CA1 is encoding the future decision of which way the animal will turn at the end or the central track. However, it is important to note that the identification of the correct choice on this task is not generated in the hippocampus as part of spatial processing (Ainge, van der Meer, Langston, & Wood, 2007). Rather, CA1 is representing the knowledge of current state provided by the prefrontal cortex via the thalamus (Ito et al., 2015). Corresponding to the understanding of this rate remapping as representation of current state as opposed to future choice, the rates of CA1 neurons on the alternation task correspond to the last trajectory, not to the future trajectory (Ji & Wilson, 2008), although see others including (Ferbinteanu & Shapiro, 2003) for similar tasks with coding of future trajectory.

In the Sensory/CA3 task, the phase dependence of rate remapping was not as clear. There was no significant phase preference of the firing rate difference across conditions (Figure 6d), nor was there a shift in preferred theta phase of spiking across conditions (Figure 6f). It is possible that we were unable to observe a difference in rate remapping in the CA3 data between the two halves of theta because of the relative weakness of rate remapping in the Sensory/CA3 task (Figure 1D). Another possibility is that rate remapping and phase precession are simply not expressed as robustly until CA1, in line with previous work showing weaker phase precession in CA3 than in CA1 (Mankin et al., 2015; Mizuseki et al., 2012). Alternatively, it may be that rate remapping in the Sensory/CA3 task occurs uniformly at all theta phases, implying that the sensory information is being represented during the mind-travel portion of the theta cycle as well as the representation of current experience. This possibility would allow for predictions of associations with upcoming locations to be recalled. An experiment to test this possibility would involve changes in the associations with upcoming locations. For example, if only half of the track was white, then one could compare rate remapping during the parts of the place field occurring under either sensory condition.

4.6 | Function of rate remapping?

One interesting point to be emphasized is the diversity of types of information represented in rate remapping. One might expect that trajectory might be represented in hippocampal place cells as a highly task-relevant factor. The sensory change of track color from black to white, which was totally irrelevant to the task being performed might not seem worth representing, although the novelty of the white track is worth noting. Despite the irrelevance of track color to the task, 30% of CA3 cells had significantly different firing rates under the two conditions in the sensory task. What can be taken from this is that even task-irrelevant aspects of the environment are represented in the rates of place cells, emphasizing the nontrivial nature of hippocampal representation.

What is the importance of representation of current state in all of its nuance during rate remapping? We believe the reason for this representation is that the hippocampus must represent current context so that any occurrences experienced can be bound to the correct context in its entirety, containing both sensorily experienced and

internally inferred information about the state of the world. Since the animal does not know beforehand which aspects of the experience will be relevant, many different aspects of the experience must be represented. Internally generated task information in the Internal/CA1 task should be thought of as representation of a "hidden state" of the world and not as representation of action plans: rate remapping represents what is known about the world, not what is predicted. Questions remain on how nonspatial information is encoded during the predictive firing during mind-travel (phase precession/theta sequences).

The alternation of rate remapping and phase precession, or alternatively encoding and recall, during the two halves of theta allows for the usage of past knowledge while nearly simultaneously doing what is necessary for learning to occur for future performance.

ACKNOWLEDGMENTS

Thank you to Simona Dalin and Magdalene Schlesiger for helpful comments on this manuscript and to Timothy O'Leary for analysis suggestions.

CONFLICT OF INTEREST

The authors declare no conflicts of interest.

ORCID

Honi Sanders https://orcid.org/0000-0001-9018-2001
Daoyun Ji https://orcid.org/0000-0003-4115-5888
Takuya Sasaki https://orcid.org/0000-0002-0576-7142
Jill K. Leutgeb https://orcid.org/0000-0002-2014-842X

REFERENCES

Aghajan, Z. M., Acharya, L., Moore, J. J., Cushman, J. D., Vuong, C., & Mehta, M. R. (2014). Impaired spatial selectivity and intact phase precession in two-dimensional virtual reality. *Nature Neuroscience*, *18*, 121–128.

Ainge, J. A., van der Meer, M. A., Langston, R. F., & Wood, E. R. (2007). Exploring the role of context-dependent hippocampal activity in spatial alternation behavior. *Hippocampus*, *17*, 988–1002.

Allen, K., Rawlins, J. N. P., Bannerman, D. M., & Csicsvari, J. (2012). Hippocampal place cells can encode multiple trial-dependent features through rate remapping. *Journal of Neuroscience*, *32*(42), 14752–14766.

Aronov, D., Nevers, R., & Tank, D. W. (2017). Mapping of a non-spatial dimension by the hippocampal–entorhinal circuit. *Nature*, *543*, 719–722.

Avila-Akerberg, O., Krahe, R., & Chacron, M. J. (2010). Neural heterogeneities and stimulus properties affect burst coding *in vivo*. *Neuroscience*, *168*, 300–313.

Barbieri, R., Quirk, M. C., Frank, L. M., Wilson, M. A., & Brown, E. N. (2001). Construction and analysis of non-Poisson stimulus–response models of neural spiking activity. *Journal of Neuroscience Methods*, *105*, 25–37.

Barry, C., Ginzberg, L. L., O'Keefe, J., & Burgess, N. (2012). Grid cell firing patterns signal environmental novelty by expansion. *Proceedings of the National Academy of Sciences of the United States of America*, *109*, 17687–17692.

Berens, P. (2009). CircStat: A MATLAB toolbox for circular statistics. *Journal of Statistical Software*, *31*, 1–21.

Bieri, K. W., Bobbitt, K. N., & Colgin, L. L. (2014). Slow and fast gamma rhythms coordinate different spatial coding modes in hippocampal place cells. *Neuron*, *82*, 670–681.

Bittner, K. C., Grienberger, C., Vaidya, S. P., Milstein, A. D., Macklin, J. J., Suh, J., … Magee, J. C. (2015). Conjunctive input processing drives feature selectivity in hippocampal CA1 neurons. *Nature Neuroscience*, *18*(8), 1133–1142.

Brette, R. (2015). Philosophy of the spike: Rate-based vs. spike-based theories of the brain. *Frontiers in Systems Neuroscience*, *9*, 1–14.

Buzsaki, G. (2002). Theta oscillations in the hippocampus. *Neuron*, *33*, 325–340.

Colgin, L. L., Denninger, T., Fyhn, M., Hafting, T., Bonnevie, T., Jensen, O., … Moser, E. I. (2009). Frequency of gamma oscillations routes flow of information in the hippocampus. *Nature*, *462*, 353–357.

Colgin, L. L., Moser, E. I., & Moser, M. B. (2008). Understanding memory through hippocampal remapping. *Trends in Neurosciences*, *31*, 469–477.

Eichenbaum, H., Yonelinas, A. P., & Ranganath, C. (2007). The medial temporal lobe and recognition memory. *Annual Review of Neuroscience*, *30*, 123–152.

Erdem, U. M., & Hasselmo, M. E. (2012). A goal-directed spatial navigation model using forward trajectory planning based on grid cells. *European Journal of Neuroscience*, *35*, 916–931.

Feng, T., Silva, D., & Foster, D. J. (2015). Dissociation between the experience-dependent development of hippocampal theta sequences and single-trial phase precession. *Journal of Neuroscience*, *35*, 4890–4902.

Fenton, A. A., Lytton, W. W., Barry, J. M., Lenck-Santini, P. P., Zinyuk, LE., Kubík, S., … Olypher AV (2010). Attention-like modulation of hippocampus place cell discharge. *Journal of Neuroscience*, *30*, 4613–4625.

Fenton, A. A., & Muller, R. U. (1998). Place cell discharge is extremely variable during individual passes of the rat through the firing field. *Proceedings of the National Academy of Sciences of the United States of America*, *95*, 3182–3187.

Ferbinteanu, J., & Shapiro, M. L. (2003). Prospective and retrospective memory coding in the hippocampus. *Neuron*, *40*, 1227–1239.

Foster, D. J., & Wilson, M. A. (2007). Hippocampal theta sequences. *Hippocampus*, *17*, 1093–1099.

Frank, L. M., Brown, E. N., & Wilson, M. A. (2000). Trajectory encoding in the hippocampus and entorhinal cortex. *Neuron*, *27*, 169–178.

Gautrais, J., & Thorpe, S. (1998). Rate coding versus temporal order coding: A theoretical approach. *BioSystems*, *48*, 57–65.

Hafting, T., Fyhn, M., Bonnevie, T., Moser, M. B., & Moser, E. I. (2008). Hippocampus-independent phase precession in entorhinal grid cells. *Nature*, *453*, 1248–1252.

Harris, K. D., Henze, D. A., Hirase, H., Leinekugel, X., Dragoi, G., Czurkó, A., & Buzsáki, G. (2002). Spike train dynamics predicts theta-related phase precession in hippocampal pyramidal cells. *Nature*, *417*, 738–741.

Harvey, C. D., Collman, F., D. A, D., & Tank, D. W. (2009). Intracellular dynamics of hippocampal place cells during virtual navigation. *Nature*, *461*, 941–946.

Hasselmo, M. E., Bodelón, C., & Wyble, B. P. (2002). A proposed function for hippocampal theta rhythm: Separate phases of encoding and retrieval enhance reversal of prior learning. *Neural Computation*, *14*, 793–817.

Herkenham, M. (1978). The connections of the nucleus reuniens thalami: Evidence for a direct thalamo-hippocampal pathway in the rat. *Journal of Comparative Neurology*, *177*, 589–610.

Huxter, J. R., Burgess, N., & O'Keefe, J. (2003). Independent rate and temporal coding in hippocampal pyramidal cells. *Nature*, *425*, 828–832.

Hyman, J. M., Wyble, B. P., Goyal, V., Rossi, C. A., & Hasselmo, M. E. (2003). Stimulation in hippocampal region CA1 in behaving rats yields long-term potentiation when delivered to the peak of theta and long-term depression when delivered to the trough. *Journal of Neuroscience*, *23*, 11725–11731.

Ito, H. T., Sj, Z., Witter, M. P., Moser, E. I., & M. B., M. (2015). A prefrontalthalamohippocampal circuit for goal-directed spatial navigation. *Nature*, *522*, 50–55.

Jackson, J. C., & Redish, A. D. (2007). Network dynamics of hippocampal cell-assemblies resemble multiple spatial maps within single tasks. *Hippocampus*, *17*, 1209–1229.

Jaramillo, J., Schmidt, R., & Kempter, R. (2014). Modeling inheritance of phase precession in the hippocampal formation. *Journal of Neuroscience*, *34*, 7715–7731.

Jensen, O., & Lisman, J. E. (1996). Hippocampal CA3 region predicts memory sequences: Accounting for the phase precession of place cells. *Learning & Memory (Cold Spring Harbor, NY)*, *3*, 279–287.

Jezek, K., Henriksen, E. J., Treves, A., Moser, E. I., & Moser, M. B. (2011). Theta-paced flickering between place-cell maps in the hippocampus. *Nature*, *478*, 246–249.

Ji, D., & Wilson, M. A. (2008). Firing rate dynamics in the hippocampus induced by trajectory learning. *Journal of Neuroscience*, *28*, 4679–4689.

Kamondi, A., Acsády, L., Wang, X. J., & Buzsáki, G. (1998). Theta oscillations in somata and dendrites of hippocampal pyramidal cells *in vivo*: Activity-dependent phase-precession of action potentials. *Hippocampus*, *8*, 244–261.

Kelemen, E., & Fenton, A. A. (2016). Coordinating different representations in the hippocampus. *Neurobiology of Learning & Memory*, *129*, 50–59.

Kempter, R., Leibold, C., Buzsáki, G., Diba, K., & Schmidt, R. (2012). Quantifying circular–linear associations: Hippocampal phase precession. *Journal of Neuroscience Methods*, *207*, 113–124.

Kepecs, A., & Lisman, J. (2003). Information encoding and computation with spikes and bursts. *Network (Bristol, UK)*, *14*, 103–118.

Kubie, J. L., & Fenton, A. A. (2012). Linear look-ahead in conjunctive cells: An entorhinal mechanism for vector-based navigation.

Lengyel, M., Szatmary, Z., & Erdi, P. (2003). Dynamically detuned oscillations account for the coupled rate and temporal code of place cell firing. *Hippocampus*, *13*, 700–714.

Leutgeb, S., Leutgeb, J. K., Barnes, C. A., Moser, E. I., McNaughton, B. L., & Moser, M. B. (2005). Independent codes for spatial and episodic memory in hippocampal neuronal ensembles. *Science*, *309*, 619–623.

Lisman, J. E., & Redish, A. D. (2009). Prediction, sequences and the hippocampus. *Philosophical Transactions of the Royal Society B*, *364*, 1193–1201.

London, M., & Häusser, M. (2005). Dendritic computation. *Annual Review of Neuroscience*, *28*, 503–532.

Lu, L., Leutgeb, J. K., Tsao, A., Henriksen, E. J., Leutgeb, S., Barnes, C. A., … Moser E. I. (2013). Impaired hippocampal rate coding after lesions of the lateral entorhinal cortex. *Nature Neuroscience*, *16*, 1085–1093.

Mankin, E. A., Diehl, G. W., Sparks, F. T., Leutgeb, S., & Leutgeb, J. K. (2015). Hippocampal CA2 activity patterns change over time to a larger extent than between spatial contexts. *Neuron*, *85*, 190–202.

Mankin, E. A., Sparks, F., Slayyeh, B., Sutherland, R., Leutgeb, S., & Leutgeb, J. K. (2012). Neuronal code for extended time in the hippocampus. *Proceedings of the National Academy of Sciences*, *109*, 19462–19467.

Markus, E. J., Qin, Y. L., Leonard, B., Skaggs, W. E., McNaughton, B. L., & Barnes, C. A. (1995). Interactions between location and task affect the spatial and directional firing of hippocampal neurons. *Journal of Neuroscience*, *15*, 7079–7094.

Maurer, A. P., & McNaughton, B. L. (2007). Network and intrinsic cellular mechanisms underlying theta phase precession of hippocampal neurons. *Trends in Neurosciences*, *30*, 325–333.

Mehta, M. R., Lee, A. K., & Wilson, M. A. (2002). Role of experience and oscillations in transforming a rate code into a temporal code. *Nature*, *417*, 741–746.

Miura, K., Mainen, Z. F., & Uchida, N. (2012). Odor representations in olfactory cortex: Distributed rate coding and decorrelated population activity. *Neuron*, *74*, 1087–1098.

Mizuseki, K., Royer, S., Diba, K., & Buzsaki, G. (2012). Activity dynamics and behavioral correlates of CA3 and CA1 hippocampal pyramidal neurons. *Hippocampus*, *22*, 1659–1680.

Mizuseki, K., Sirota, A., Pastalkova, E., & Buzsáki, G. (2009). Theta oscillations provide temporal windows for local circuit computation in the entorhinal–hippocampal loop. *Neuron*, *64*, 267–280.

Muller, R. U., & Kubie, J. L. (1987). The effects of changes in the environment on the spatial firing of hippocampal complex–spike cells. *Journal of Neuroscience*, *7*, 1951–1968.

Muller, R. U., Kubie, J. L., & Ranck, J. B. (1987). Spatial firing patterns of hippocampal complex-spike cells in a fixed environment. *Journal of Neuroscience*, *7*, 1935–1950.

O'Keefe, J. (1976). Place units in the hippocampus of the freely moving rat. *Experimental Neurology*, *51*, 78–109.

O'Keefe, J., & Burgess, N. (2005). Dual phase and rate coding in hippocampal place cells: Theoretical significance and relationship to entorhinal grid cells. *Hippocampus*, *15*, 853–866.

O'Keefe, J., & Recce, M. L. (1993). Phase relationship between hippocampal place units and the EEG theta rhythm. *Hippocampus*, *3*, 317–330.

Olypher, A. V., Lánsky, P., & Fenton, A. A. (2002). Properties of the extra-positional signal in hippocampal place cell discharge derived from the overdispersion in location-specific firing. *Neuroscience*, *111*, 553–566.

Ramón y Cajal, S. (1911). *Histologie du systéme nerveux de l'homme et des vertébrées*. Paris, A Maloine.

Ranck, J. B. (1973). Studies on single neurons in dorsal hippocampal formation and septum in unrestrained rats: I. Behavioral correlates and firing repertoires. *Experimental Neurology*, *41*, 462–531.

Rangel, L. M. (2012). The encoding of spatial, temporal and affective dimensions in the dentate gyrus of the hippocampus. Ph.D. diss., UC San Diego.

Robitsek, R. J., White, J. A., & Eichenbaum, H. (2013). Place cell activation predicts subsequent memory. *Behavioural Brain Research*, *254*, 65–72.

Royer, S., Zemelman, B. V., Losonczy, A., Kim, J., Chance, F., Magee, J. C., & Buzsáaki, G. (2012). Control of timing, rate and bursts of hippocampal place cells by dendritic and somatic inhibition. *Nature Neuroscience*, *15*, 769–775.

Sanders, H., Rennó-Costa, C., Idiart, M., & Lisman, J. E. (2015). Grid cells and place cells: An integrated view of their navigational/memory function. *Trends in Neurosciences*, *38*, 763–775.

Schiller, D., Eichenbaum, H., Buffalo, E. A., Davachi, L., Foster, D. J., Leutgeb, S., & Ranganath, C. (2015). Memory and space: Towards an understanding of the cognitive map. *Journal of Neuroscience*, *35*, 13904–13911.

Schlesiger, M. I., Cannova, C. C., Boublil, B. L., Hales, J. B., Mankin, E. A., Brandon, M. P., … Leutgeb, S. (2015). The medial entorhinal cortex is necessary for temporal organization of hippocampal neuronal activity. *Nature Neuroscience*, *18*, 1123–1132.

Schomburg, E. W., Fernández-Ruiz, A., Mizuseki, K., Beréenyi, A., Anastassiou, C. A., Koch, C., & Buzsaki, G. (2014). Theta phase segregation of input-specific gamma patterns in entorhinal–hippocampal networks. *Neuron*, *84*(2), 470–485.

Scoville, W., & Milner, B. (1957). Loss of recent memory after bilateral hippocampal lesions. *Journal of Neurology, Neurosurgery & Psychiatry*, *20*, 11–21.

Shadlen, M. N., & Newsome, W. T. (1994). Noise, neural codes and cortical organization. *Current Opinion in Neurobiology*, *4*, 569–579.

Siegle, J. H., & Wilson, M. A. (2014). Enhancement of encoding and retrieval functions through theta phase-specific manipulation of hippocampus. *ELife*, *2014*, 1–18.

Skaggs, W. E., McNaughton, B. L., Wilson, M. A., & Barnes, C. A. (1996). Theta phase precession in hippocampal neuronal populations and the compression of temporal sequences. *Hippocampus*, *6*, 149–172.

Softky, W. R. (1995). Simple codes versus efficient codes. *Current Opinion in Neurobiology*, *5*, 239–247.

Steward, O., & Scoville, S. A. (1976). Cells of origin of entorhinal cortical afferents to the hippocampus and fascia dentata of the rat. *Journal of Comparative Neurology*, *169*, 347–370.

Terrazas, A., Krause, M., Lipa, P., Gothard, K. M., C. A, B., & McNaughton, B. L. (2005). Self-motion and the hippocampal spatial metric. *Journal of Neuroscience*, *25*, 8085–8096.

Witter., M. P. (2010). Connectivity of the hippocampus. In: V. Cutsuridis, B. Graham, S. Cobb, & I. Vida (Eds.), *Hippocampal microcircuits* (Chap. 1, pp. 5–26). New York, NY: Springer.

Wood, E. R., Dudchenko, P. A., Robitsek, R. J., & Eichenbaum, H. (2000). Hippocampal neurons encode information about different types of memory episodes occurring in the same location. *Neuron*, *27*, 623–633.

Wu, Y. (2012). In search of lost time Ph.D. diss., University of Waterloo.

Yamaguchi, Y., Aota, Y., McNaughton, B. L., & Lipa, P. (2002). Bimodality of theta phase precession in hippocampal place cells in freely running rats. *Journal of Neurophysiology*, *87*, 2629–2642.

Zheng, C., Bieri, K. W., Hsiao, Y. T., & Colgin, L. L. (2016). Spatial sequence coding differs during slow and fast gamma rhythms in the hippocampus. *Neuron*, *89*, 398–408.

How to cite this article: Sanders H, Ji D, Sasaki T, Leutgeb JK, Wilson MA, Lisman JE. Temporal coding and rate remapping: Representation of nonspatial information in the hippocampus. *Hippocampus*. 2019;29:111–127. https://doi.org/10.1002/hipo.23020